Regular Article

ANALYTICAL AND BIOANALYTICAL CHEMISTRY RESEARCH

Published by the Iranian Chemical Society

Anal. Bioanal. Chem. Res., Vol. 4, No. 1, 141-154, June 2017.

Modification of $CoFe_2O_4$ Magnetic Nanoparticles by Dopamine and Ascorbic Acid as Anchors

Maryam Ghaemi[a], Ghodratollah Absalan[b,*] and Tayebe Pourshamsi[b]

[a]*Department of Marine Science, Iranian National Institute for Oceanography and Atmospheric Science, No. 3, Etemadzadeh St., Fatemi Ave., Tehran, 1411813389, IR Iran*

[b]*Professor Massoumi Laboratory, Department of Chemistry, Faculty of Sciences, Shiraz University, Shiraz 71454, Iran*

(Received 26 July 2016, Accepted 2 March 2017)

$CoFe_2O_4$ magnetic nanoparticles were modified by dopamine (DA) and ascorbic acid (AA) as anchors. Separation of the DA and AA using $CoFe_2O_4$ magnetic nanoparticles have been studied by investigating the effects of pH, concentration of the DA and AA, amount of adsorbents, contact time, ionic strength and temperature. The mechanism of adsorption was also studied. The adsorption of DA and AA to the $CoFe_2O_4$ magnetic nanoparticles could be described by Langmuir-type adsorption isotherms. The effective surface area of the $CoFe_2O_4$ nanoparticles was 53.55 m^2 g^{-1} and 109.81 m^2 g^{-1}, respectively, for DA and AA. The maximum adsorption capacities were 28.98 and 72.99 mg of enediol per gram of adsorbent for DA and AA, respectively. With the help of adsorption isotherm, thermodynamic parameters such as free energy, enthalpy, and entropy have been calculated. The adsorption of DA onto $CoFe_2O_4$ is exothermic, though the temperature effect was negligible for adsorption of AA. On the basis of pseudo-first-order and pseudo-second-order kinetic equations different kinetic parameters were obtained. DA and AA can be desorbed from $CoFe_2O_4$ using concentrated imidazole as an eluent.

Keywords: Magnetic nanoparticle, Adsorption, Dopamine, Ascorbic acid

INTRODUCTION

Nanoparticles (NPs) of transition-metal oxides have generated vast interest in recent years because of their unique size and physical properties that are not observed for bulk materials [1]. Magnetic nanoparticles are flourishing in biotechnology and medical applications due to their relative inertness, superior magnetic properties, high biocompatibility, and the apparent simplicity of post-synthesis surface functionalization. Moreover, they have unique chemistry with enhanced chemical reactivity, catalytic activity, and specific bindings [2-4]. They have been used as contrast agents in magnetic resonance imaging (MRI) [5], and were applied in ferrofluid technology for MRI monitoring in hypothermia [6]. Their other applications include cancer tumor detection *via* SQUID magnetometry [7], selective sorption of biomolecules [8-10], metal ions [11] and dyes [12]. In this regard, controlling the surface chemistry, shape, size, and stability of nanomaterials have gained considerable attention.

Stability of the bonding between functional molecules and nanoparticles is crucial because the particle is the key to tracking or targeting treatments that the functional molecule is to perform in most medical applications. Iron oxide nanoparticles are typically stabilized with dispersants if used for biomedical applications [13]. According to the published methods, the iron oxide could be modified by carboxylate [14] or enediol ligands (such as dopamine and ascorbic acid) [15-23]. Since catechols such as dopamine have high affinity toward a broad range of oxides [24],

*Corresponding author. E-mail: absalan@susc.ac.ir

they are applicable to stabilize oxide nanoparticles. Thus, these catechol-based dispersants might pave the way for a variety of new applications of oxide nanoparticles. Dopamine (DA) has sparked a great interest as capping agent due to the stability and strength of the resultant five-membered metallocycle chelate and the ease at which it can be functionalized through amide bonds with other molecules of interest.

Dopamine, which is the most important neurotransmitter among the catecholamines, plays an important role in the function of central nervous, renal, hormonal and cardiovascular systems. The change of DA has been proved to be a very effective route toward brain tissues, and the loss of DA-containing neurons may result in serious diseases, such as Parkinson [25].

Among magnetic nanoparticles, $CoFe_2O_4$ has attracted considerable attention due to its unique physical properties such as high curie temperature, large magneto crystalline anisotropy, high coercivity, moderate saturation magnetization, higher magnetostriction than metallic Fe or Ni [26], excellent chemical stability and mechanical hardness [27]. Because of the wide applicability of cobalt ferrite nanoparticles in biological research, the ease of linking other biomolecules to cobalt ferrite surfaces through a versatile anchor, such as dopamine (DA) and ascorbic acid (AA), should lead to useful applications of these nanostructures in several areas, *e.g.*, cell biology, biotechnology, and environmental monitoring. It should be mentioned that there are different sorbents for adsorption of DA and AA, including carbon-fiber electrodes by 2,6-anthraquinone disulfonic acid (2,6-AQDS), 4-carboxyphenyl or catechols [28], nanocrystalline metal oxide particles (TiO_2, Fe_2O_3 and ZrO_2) [23], Fe_2O_3 nanoparticles [15,16], and anatase TiO_2 (101) single crystals [29].

To the best of our knowledge, no such studies in the field of analytical chemistry on the adsorption of enediol ligands on $CoFe_2O_4$ magnetic nanoparticles have been reported yet. The aim of this study is modification of $CoFe_2O_4$ magnetic nanoparticles by dopamine and ascorbic acid as anchors and investigation of the mechanism and predominant factors controlling the adsorption of DA and AA onto these nanoparticles.

EXPERIMENTAL

Chemicals and Reagents

Analytical grades dopamine (3-hydroxytyramine hydrochloride), sodium hydroxide, hydrochloric acid, imidazol, $FeCl_3.6H_2O$ and $CoCl_2.4H_2O$ were purchased from Merck. L(+)-ascorbic acid was purchased from Riedel-de Haën. Stock solutions (1000 mg l^{-1}) of DA and AA were prepared. Scheme 1 depicts chemical structures for two enediol ligands, ascorbic acid and dopamine.

Instrumentation

A UV-Vis spectrophotometer (Pharmacia Biotech) equipped with a 1-cm quartz cell was used for recording the visible spectra and absorbance measurements. A Metrohm 780 pH meter was used for monitoring the pH values. A water ultrasonicator (Model CD-4800, China) was used to disperse the nanoparticles in solution and a supermagnet Nd-Fe-B (1.4 T, 10 × 5 × 2 cm) was used. Transmission electron microscope (Philips CM 10TEM) was used for recording the TEM images. The TEM images were analyzed by "Image J software". Vibrating sample magnetometer (VSM, PPMS-9T) was used for measuring the magnetization curve of the nanoparticles.

Preparation of $CoFe_2O_4$ Nanoparticles

Cobalt ferrite nanoparticles were synthesized by a co-precipitation technique reported in the literature [30]. Briefly, aliquot of 80 ml of an aqueous solution containing 0.11 M Fe^{3+} and 0.055 M Co^{2+} was continuously added into a reaction vessel containing 150 ml of boiling 0.725 M NaOH under continuous mechanical stirring at 500 rpm. The contact time of 2 h was performed for dehydration and atomic rearrangement and conversion of the intermediate hydroxide phase into the spinel structure. The produced $CoFe_2O_4$ nanoparticles were rinsed three times, each time with 50 ml distilled water and then were magnetically separated. Figure 1 is a representative TEM image of $CoFe_2O_4$ nanoparticles. The average diameter of $CoFe_2O_4$ nanoparticles was about ~10 nm. The magnetic property of $CoFe_2O_4$ was measured out from -10000 Oe to 10000 Oe at room temperature using VSM magnetometer, Fig. 2. It can be seen that the magnetization curve appears as an S-shape

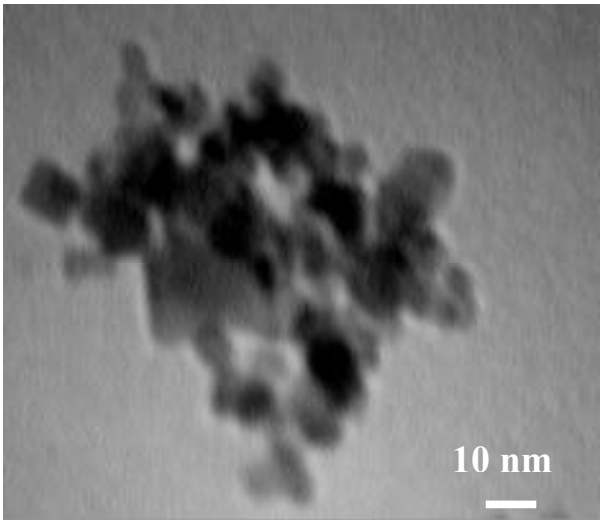

Fig. 1. The TEM image of $CoFe_2O_4$ nanoparticles.

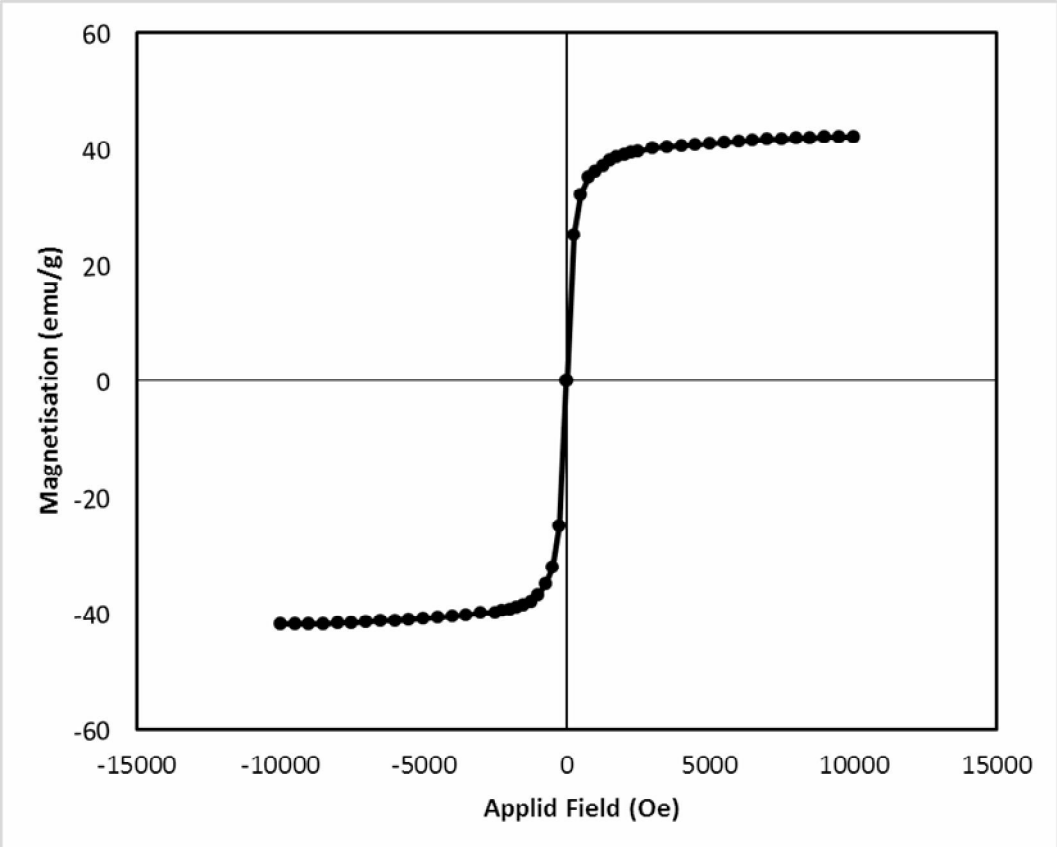

Fig. 2. The Magnetization curve of $CoFe_2O_4$ nanoparticles.

over the applied magnetic field. The value of the saturation magnetization (Ms) of the $CoFe_2O_4$ is 41.9 emu g^{-1}. The field-dependent magnetization curve shows negligible remanence and coercivity, indicating superparamagnetic behavior of the nanoparticles at room temperature.

Procedure for Adsorption of Dopamine and Ascorbic Acid

Adsorption experiments with the synthesized $CoFe_2O_4$ nanoparticles were carried out using batch method under magnetic stirring. Each experiment consisted of preparing a 5.0 ml of DA and AA solution with a desired initial concentration (10.0-80.0 mg l^{-1} for DA and 10.0-120.0 mg l^{-1} for AA) and pH 3.0-10.0, by diluting the stock solutions with distilled water, and transferring it into the individual beaker on the magnetic stirrer. A known dosage of nano-$CoFe_2O_4$ in the range of 5.0-13.0 mg was then added to the solution. After the mixing time elapsed (2.0-30.0 min), the magnetic particles were separated magnetically. The DA and AA concentrations in the supernatant were measured by UV-Vis spectrometer, and the equilibrium adsorption amount was calculated according to Eq. (1) [31].

$$q_e = \frac{(C_0 - C_e)V}{m} \quad (1)$$

where C_0 and C_e, respectively, represent the initial and final (after adsorption) DA and AA concentrations (in mg l^{-1}) in the aqueous phase, V is the volume of DA and AA solution used (in l), and m is the mass of adsorbent used (in g). All tests were performed in duplicate at ambient temperature.

RESULTS AND DISCUSSION

Effect of Solution pH

To investigate the effect of pH on the adsorption of enediols, DA and AA, a pH range of 3.0-10.0 with a stirring time of 15.0 min, were chosen. The pH of the test solution was adjusted by HCl and NaOH solutions. The initial concentrations of both DA and AA were 25.0 mg l^{-1} and the amount of the adsorbent was 12.0 mg for all batch experiments. Figure 3 presents the effect of pH on the adsorption percentage of DA and AA. As shown in this figure, the adsorption percentage changed from 83.6% to 79.2% for DA and from 96.2% to 82.7% for AA when pH increased from 3.0 to 10.0. It should be mentioned that the experiment was not performed at pHs lower than 2.5 as the nanoparticles dissolve.

As shown in Scheme 2, the interaction between nanoparticles and enediols is due to the formation of coordination bonds between either cobalt and/or iron ions of the nanoparticles and the ortho-substituted hydroxyl groups of the enediols [23,32]. The difference in binding affinities of DA and AA might be related to their different pK_a values. The adsorption percentage of AA was high in the pH range of 3.0-7.0 (Fig. 3), mainly due to the complexation of the ortho-substituted hydroxyl groups of the furan ring of AA with metal ions in nanoparticles. It should be mentioned that diprotic form of AA dominates up to a pH value of 4.1 (pK_{a1} AA = 4.04). At pHs more than 4.1, the monoprotic form of AA (a negatively-charged species) is the predominant species. However, $CoFe_2O_4$ particles become negatively charged (pH_{zpc} is 7.4) at basic condition and consequently, adsorption percentage is expected to reduce due to electrostatic repulsion between negatively-charged AA and negatively-charged $CoFe_2O_4$ nanoparticles at higher basic solution.

At pHs below 4.0, adsorption percentage of DA (pK_{a1} = 8.88) is lower due to its electrostatic repulsion with the positively-charged $CoFe_2O_4$ surface (pH_{zpc} is 7.4). Adsorption of DA, in a fully protonated form, is slow on $CoFe_2O_4$ nanoparticles surfaces though its value does not change. Deprotonation of DA upon adsorption to $CoFe_2O_4$ nanoparticles is in a good agreement with data reported in the literature where protons from alcohols of catechols have been reported to be dissociated upon being adsorbed on TiO_2 and Fe_3O_4 [23,33,34]. Ascorbic acid has a lower pK_{a1} (pK_{a1} = 4.04), compared to DA (pK_{a1} = 8.88), therefore, adsorption percentage of AA would be higher than that of DA in the more acidic conditions, as shown in Fig. 3.

Effect of Nanoparticle Dosage

The effect of $CoFe_2O_4$ quantity on adsorption of DA and AA was investigated in batch technique by adding

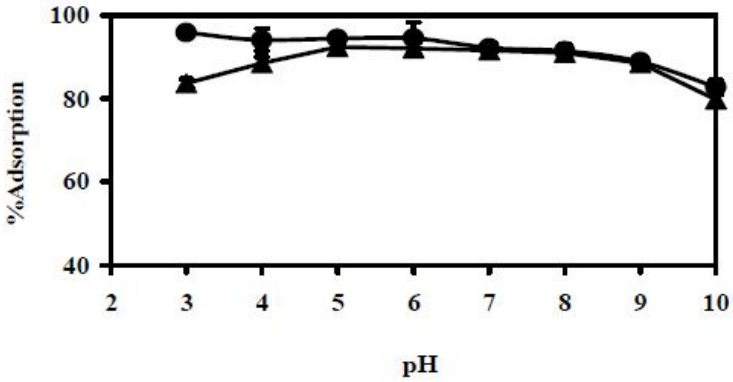

Fig. 3. Effect of pH of solutions on adsorption of AA (●) and DA (▲). Experimental conditions: $CoFe_2O_4$ dosage of 12.0 mg; initial concentrations 25.0 mg l^{-1}; stirring time of 15 min (at 500 rpm). The error bars correspond to the percentage of average deviations.

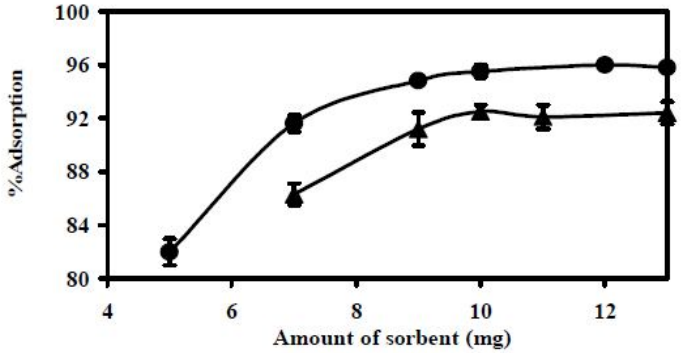

Fig. 4. Effect of $CoFe_2O_4$ dosage on adsorption percentage of AA (●) and DA (▲). Experimental conditions: initial AA and DA concentrations of 25.0 mg l^{-1}; stirring time of 15 min (at 500 rpm); optimum pH of 3.0 for AA and 6.5 for DA. The error bars correspond to the percentage of average deviations.

various amounts of the adsorbent (5.0-13.0 mg) into beakers containing 5.0 ml of individual DA and AA solution with initial concentrations of 25 mg l^{-1} at pH 3.0 for AA and at pH 6.5 for DA. By increasing the amount of adsorbent up to a value of 10.0 mg, the adsorption percentage increased (Fig. 4) as more active sites of the adsorbent were available for adsorbing DA and AA molecules. Further addition of the adsorbent did not show any significant change in the adsorption percentage. Thus, 12.0 mg of the nanoparticles was chosen as the optimum amount for performing the following steps of the optimization procedure.

Effect of Enediol Concentration

In order to find the required concentrations of enediols that must be used in the optimization procedure, the adsorption of different concentrations of DA and AA, in the range of 10.0-80.0 mg l^{-1} DA at pH 6.5 and 10.0-120.0 mg l^{-1} AA at pH 3.0 was studied individually. The experimental results of this study, shown in Fig. 5, revealed that the adsorption sites of the nanoparticles became saturated almost at DA concentration of more than 40 mg l^{-1} and at AA concentration of more than 100 mg l^{-1} at the performed experimental conditions. According to Fig. 5, $CoFe_2O_4$ nanoparticles showed greater capacity for adsorption of AA. A concentration of 25 mg l^{-1}, for each enediol, was selected

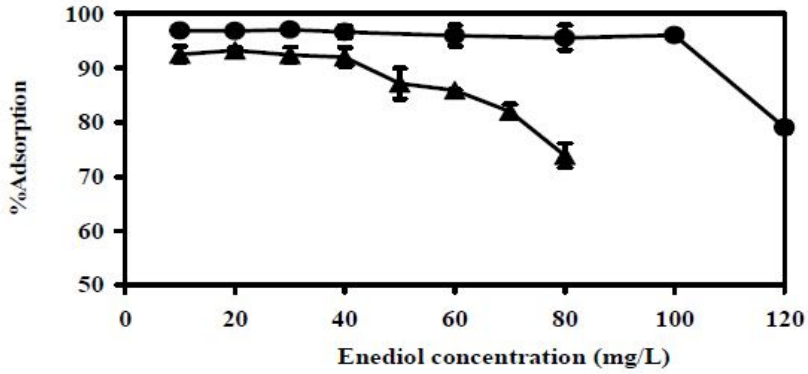

Fig. 5. Dependency of the adsorption percentage of AA (●) and DA (▲) on their initial concentrations. Experimental conditions: $CoFe_2O_4$ dosage of 12.0 mg; optimum pH of 3.0 for AA and 6.5 for DA; stirring time of 15 min (at 500 rpm). The error bars correspond to the percentage of average deviations.

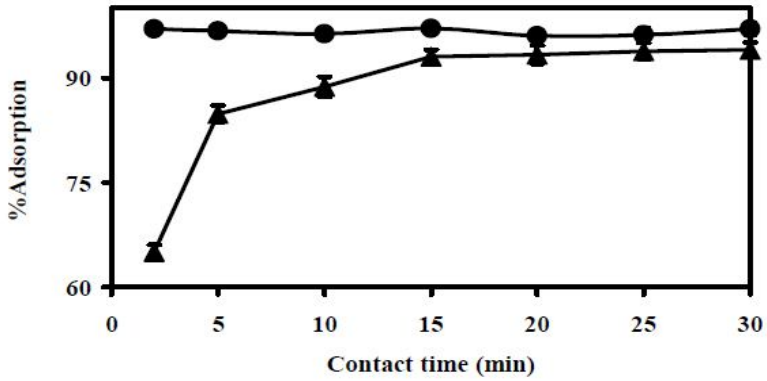

Fig. 6. Effect of contact time on adsorption of AA (●) and DA (▲) by $CoFe_2O_4$ nanoparticles. Experimental conditions: $CoFe_2O_4$ dosages of 12.0 mg; initial concentrations of 25.0 mg l^{-1} for AA and DA; optimum pH of 3.0 for AA and 6.5 for DA. The error bars correspond to percentage of average deviations.

for following the optimization procedure.

Effect of Contact Time

The effect of contact (stirring or agitation) time between nanoparticles and enediols was investigated for 25 mg l^{-1} of individual DA and AA solution. Figure 6 shows the adsorption percentage of both DA and AA as a function of stirring time (at 500 rpm) in the time period of 2.0 to 30.0 min. The results indicated that the adsorption process started immediately upon addition of $CoFe_2O_4$ to the sample solution containing AA and almost 97.0% of AA was adsorbed within 2.0 min. The adsorption of 25 mg l^{-1} of DA was found to be quantitatively completed within 15.0 min. Thus, a contact time of 2.0 min was found to be appropriate in order to reduce the possible interfering effect of AA in adsorption of DA. The contact time obtained in this study was found to be shorter than most of the reported values for DA and AA adsorption by other adsorbents [18].

Effect of Solution Temperature

The effect of temperature on the adsorptions of 25 mg l^{-1} of either DA or AA solution was investigated at pH 3.0 for

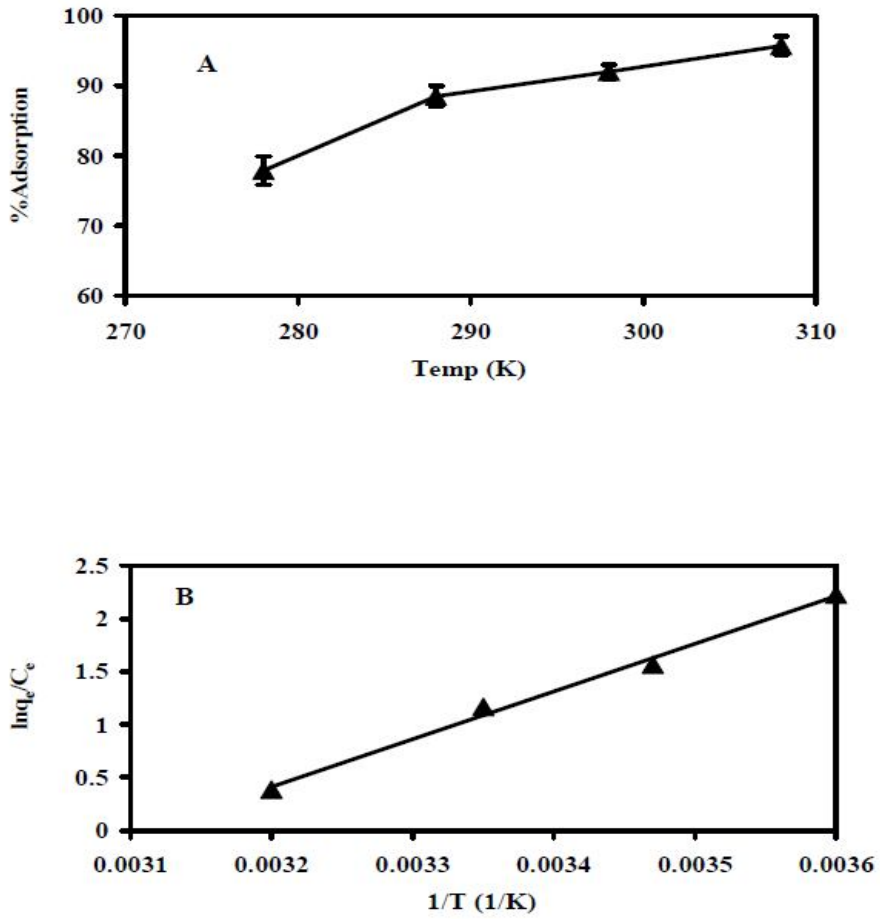

Fig. 7. (A), Effect of temperature on the adsorption of DA by $CoFe_2O_4$ nanoparticles; and (B), $\ln(q_e/C_e)$ *vs*. 1/T plots for DA.

AA and pH 6.5 for DA while a stirring time of 15.0 min (at 500 rpm) was performed. Figure 7A shows the variation of the adsorption percentage of DA as a function of temperature in the range of 278-308 K. It was found that the adsorption of DA was controlled by temperature, though the temperature effect was negligible for the adsorption of AA.

The linear plot of $\ln(q_e/C_e)$ *vs*. 1/T is shown in Fig. 7B. The changes of enthalpy (ΔH) and entropy (ΔS) at 278-308 K could be determined from the slope and intercept of the line, respectively. Table 1 shows the thermodynamic parameters for the adsorption of DA onto $CoFe_2O_4$ nanoparticles. The free energy change (ΔG) for adsorption of DA onto $CoFe_2O_4$ is negative, at the studied range of temperature, indicating the spontaneity nature of the adsorption process. The negative value of enthalpy change for adsorption of DA confirms the exothermic nature of the process. Since both ΔH and ΔS as well as the ΔG term are negative, this indicates that the $T\Delta S$ term must be less negative than ΔH indicating that the adsorption process is driven by enthalpy change.

Effect of Solution Ionic Strength

The effect of ionic strength on the adsorption percentage of DA and AA was investigated under the optimum experimental conditions in batch technique. Selected concentrations of KCl, in the range of 0.05-0.5 M, were

Table 1. Thermodynamic Parameters for Adsorption of Dopamine onto $CoFe_2O_4$ Nanoparticles

ΔS_0^T (J mol^{-1} K^{-1})	ΔH_0^T (kJ mol^{-1})	ΔG_0^T (kJ mol^{-1})			
		278 K	288 K	298 K	308 K
-116.41	-37.45	-5.09	-3.92	-2.76	-1.59

Table 2. Adsorption Isotherm Parameters for Adsorption of DA and AA onto $CoFe_2O_4$ Nanoparticles Surfaces

	Langmuir model				Freundlich model		
	q_{max} (mg g^{-1})	R_L	Effective surface area (m^2 g^{-1})	R^2	K_F (mg g^{-1})	n (g l^{-1})	R^2
DA	28.98	0.12	53.55	0.99	9.32	2.40	0.92
AA	72.99	0.95	109.81	0.94	11.57	1.94	0.83

Table 3. Kinetic Parameters for the Adsorption of DA onto $CoFe_2O_4$ Nanoparticles

Pseudo-first-order model			Pseudo-second-order model		
k_1 (1 min^{-1})	q_e (mg g^{-1})	R^2	k_2 (g mg^{-1} min^{-1})	q_e (mg g^{-1})	R^2
0.188	2.78	0.978	0.141	10.04	0.999

added into individual beakers containing 5.0 ml of 25.0 mg l^{-1} of the studied enediols. After elapsing the mixing time, the $CoFe_2O_4$ nanoparticles were magnetically separated and the solutions were analyzed for the residual enediols. The adsorption percentage was not significantly affected with increasing KCl concentration. The ionic strength-independent adsorption of DA and AA on the $CoFe_2O_4$ nanoparticles indicated that the sorption mechanism could be an inner-surface complexation at the applied experimental conditions as also reported by other researchers [35,36]. For instance, Chen *et al.* reported that in their work, the sorption of europium on attapulgite was independent of $NaClO_4$ concentration suggesting that the sorption was mainly dominated by inner-sphere surface complexation [37].

Adsorption Isotherm Modeling

The adsorption isotherms of DA and AA were analyzed by Langmuir and Freundlich isotherm models. The main

consideration of the Langmuir isotherm is sorption that takes place at specific homogeneous sites within the adsorbent, indicating a monolayer adsorption process. The linearized Langmuir isotherm is expressed as [38]:

$$\frac{C_e}{q_e} = \frac{1}{bq_{\max}} + \frac{C_e}{q_{\max}} \quad (2)$$

where C_e shows the equilibrium concentration of DA and AA (mg l^{-1}) and q_e is the amount of DA and AA adsorbed (mg) per gram $CoFe_2O_4$. The q_{max} is the surface concentration at monolayer coverage in mg g^{-1} and illustrates the maximum value of q_e that can be attained as C_e is increased. The b parameter is a coefficient related to the energy of adsorption and increases with increasing the strength of the adsorption bond. Values of q_{max} and b are determined from the linear regression plot of (C_e/q_e) *vs.* C_e.

A constant separation factor as described by Hall *et al.* [39] called "constant separation factor" or "equilibrium parameter" (R_L), is defined as

$$R_L = \frac{1}{1+bC_0} \quad (3)$$

R_L informs us about the favorability of the sorption process. For a favorable reaction process: $0 < R_L < 1$, whereas for an irreversible case the value of R_L is zero. For a linear case, R_L is 1; and for an unfavorable reaction, R_L is > 1. The values of R_L for DA and AA fall between 0 and 1, which is consistent with the favorability of the adsorption process.

The Freundlich adsorption isotherm, which is generally based on multilayer adsorption on heterogeneous surface, holds the assumption that the adsorption sites are distributed exponentially with respect to the heat of adsorption. The Freundlich isotherm can be expressed as [40]:

$$\log q_e = \log K_F + \frac{1}{n}\log C_e \quad (4)$$

where K_F and n are the constants from the Freundlich equation representing the capacity of the adsorbent for the adsorbate and the reaction order, respectively. The value of n in the range of 1-10 denotes favorable adsorption and could be find out from the linear regression plot of $\log q_e$ *vs.* $\log C_e$.

Plots of experimental results of Langmuir and Freundlich isotherm models are shown in Figures 8 and 9. The calculated values of the Langmuir and Freundlich model parameters are given in Table 2. The comparison of correlation coefficients (R^2) of the linearized forms indicated that the Langmuir model yields a better fit for the experimental equilibrium adsorption data than the Freundlich model. This suggests the formation of monolayer coverage of the surface of $CoFe_2O_4$ nanoparticles by DA and AA molecules. Similar findings are reported for binding enediol ligands on TiO_2 and Fe_2O_3 nanoparticle surfaces using Langmuir adsorption isotherm [15,23]. The calculated effective surface area of the $CoFe_2O_4$ nanoparticles for DA and AA adsorption were 53.55 m^2 g^{-1} and 109.81 m^2 g^{-1}, respectively. The Langmuir-isotherm plot was used to determine the effective surface area per gram of the nanoparticles [41]. To do this, the reciprocal of the slope of the Langmuir plot and the adsorbate molecular weight was multiplied by the Avogadro number and the cross sectional area of the adsorbate molecule [41]. The cross sectional areas of DA and AA molecules are 0.47 nm^2/molecule and 0.44 nm^2/molecule, respectively [42].

Kinetic of Adsorption

The kinetics of adsorption describes the solute uptake rate, which in turn governs the residence time of the adsorption reaction. It is one of the important characteristics in defining the efficiency of adsorption. In this study, pseudo-first-order and pseudo-second-order models were applied to examine the controlling mechanism of DA adsorption from aqueous solutions.

The pseudo-first -order Lagergren equation is given by [43]:

$$\log(q_e - q_t) = \log q_e - \frac{k_1 t}{2.303} \quad (5)$$

where k_1 is the pseudo-first-order rate constant (1 min^{-1}), q_e and q_t are the amounts of DA adsorbed (mg g^{-1}) at equilibrium and at time t (in min). The pseudo-second-order model can be expressed as [44]:

$$\frac{t}{q_t} = \frac{1}{k_2 q_e^{\,2}} + \frac{t}{q_e} \quad (6)$$

where k_2 (g mg^{-1} min^{-1}) is the rate constant of pseudo-second

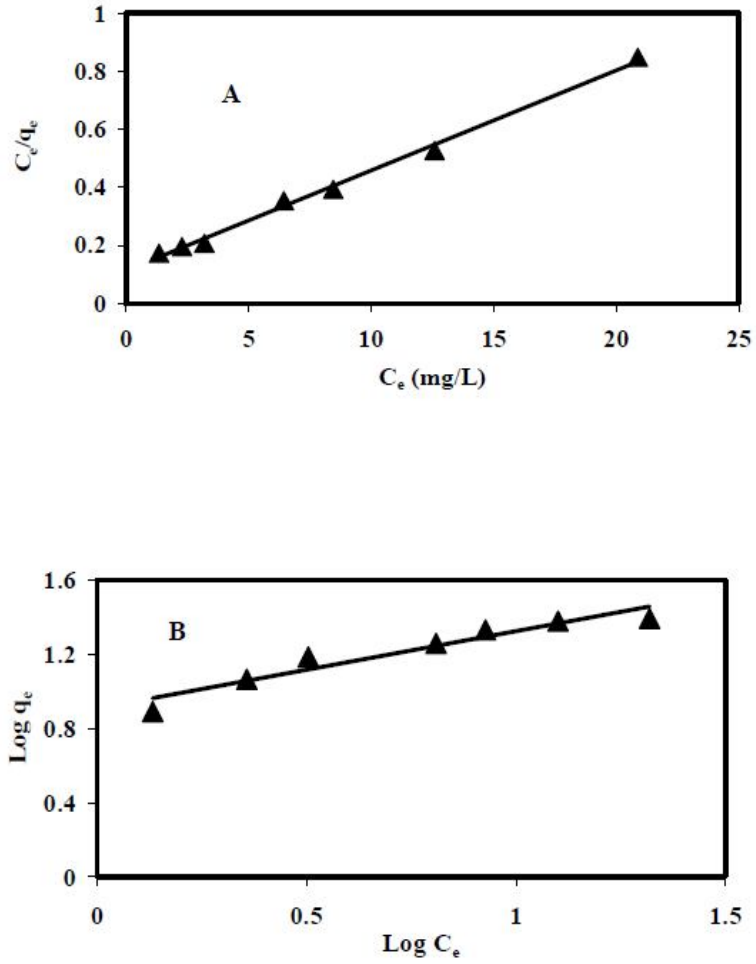

Fig. 8. (A), Langmuir isotherm plots; (B), Freundlich isotherm plots for adsorption of DA onto $CoFe_2O_4$ nanoparticles.

adsorption. Plots of experimental results of the two models are shown in Fig. 10. Kinetic constants obtained by linear regression for the two models are listed in Table 3. As shown in this table, higher values of R^2 were obtained for pseudo-second-order than for pseudo-first-order adsorption rate models, indicating that the adsorption rates of DA onto $CoFe_2O_4$ nanoparticles can be more appropriately described using the pseudo-second-order rate model.

Desorption Studies

Desorption studies help to elucidate the mechanism of adsorption and recovery of the adsorbate and adsorbent. DA and AA recoveries from the nanoparticles were conducted by incubating the nanoparticles in concentrated imidazole. The particles were collected magnetically from the eluent. In this study, more than 90% of DA and AA could be desorbed and recovered by 5.0 ml of the concentrated imidazole in 20 min. Desorption of DA and AA from the surface of nanoparticles could be interpreted on the basis of molecular interaction of the proton-donating group such as NH and OH of AA and DA via hydrogen bonding with nitrogen atoms in imidazole [45].

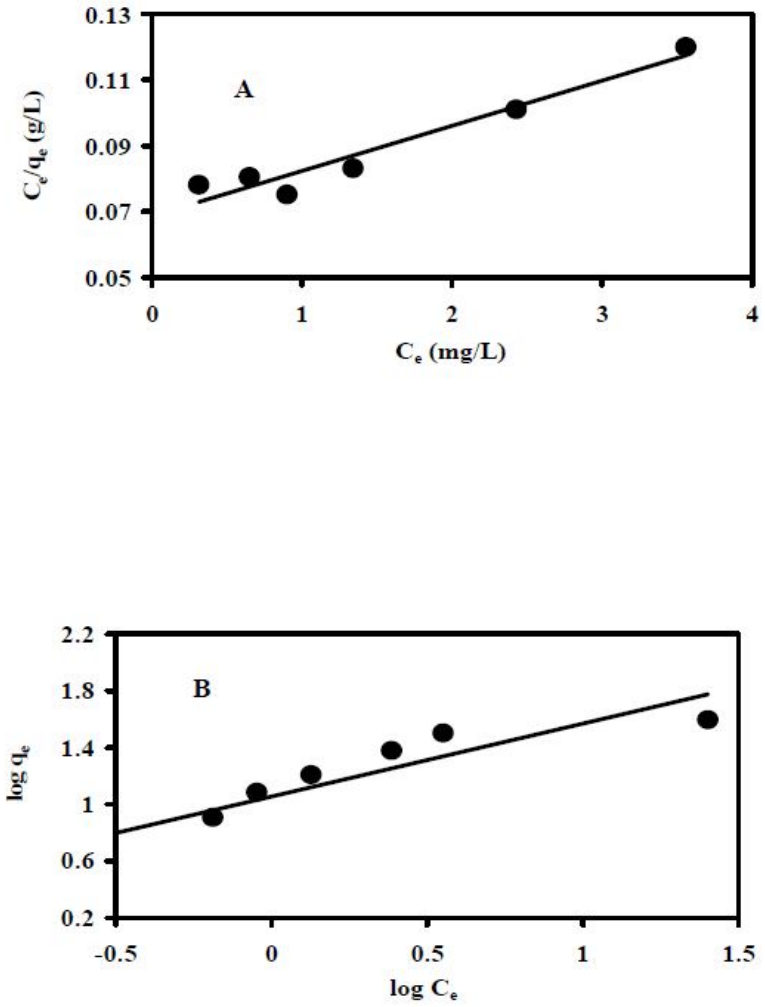

Fig. 9. (A), Langmuir isotherm plots; (B), Freundlich isotherm plots for adsorption of AA onto $CoFe_2O_4$ nanoparticles.

CONCLUSIONS

Because enediols are known to have high affinity toward a broad range of oxides, they could be applicable for stabilizing oxide nanoparticles. This procedure demonstrates an efficient, fast, simple, and inexpensive protocol for modification of $CoFe_2O_4$ magnetic nanoparticles with DA and AA which could be performed in any laboratory without using sophisticated equipment. The method offers a novel way to anchor biomolecules on $CoFe_2O_4$ nanoparticles in order to produce new biomedical nanomaterials and nanosensors. The adsorption process followed the Langmuir isotherm model and the kinetic data were appropriately fitted to a second-order adsorption rate. The performance of $CoFe_2O_4$ nanoparticles compared with other previously reported studies is shown in Table 4.

ACKNOWLEDGEMENTS

The authors wish to acknowledge the support of this work by Shiraz University Research Council.

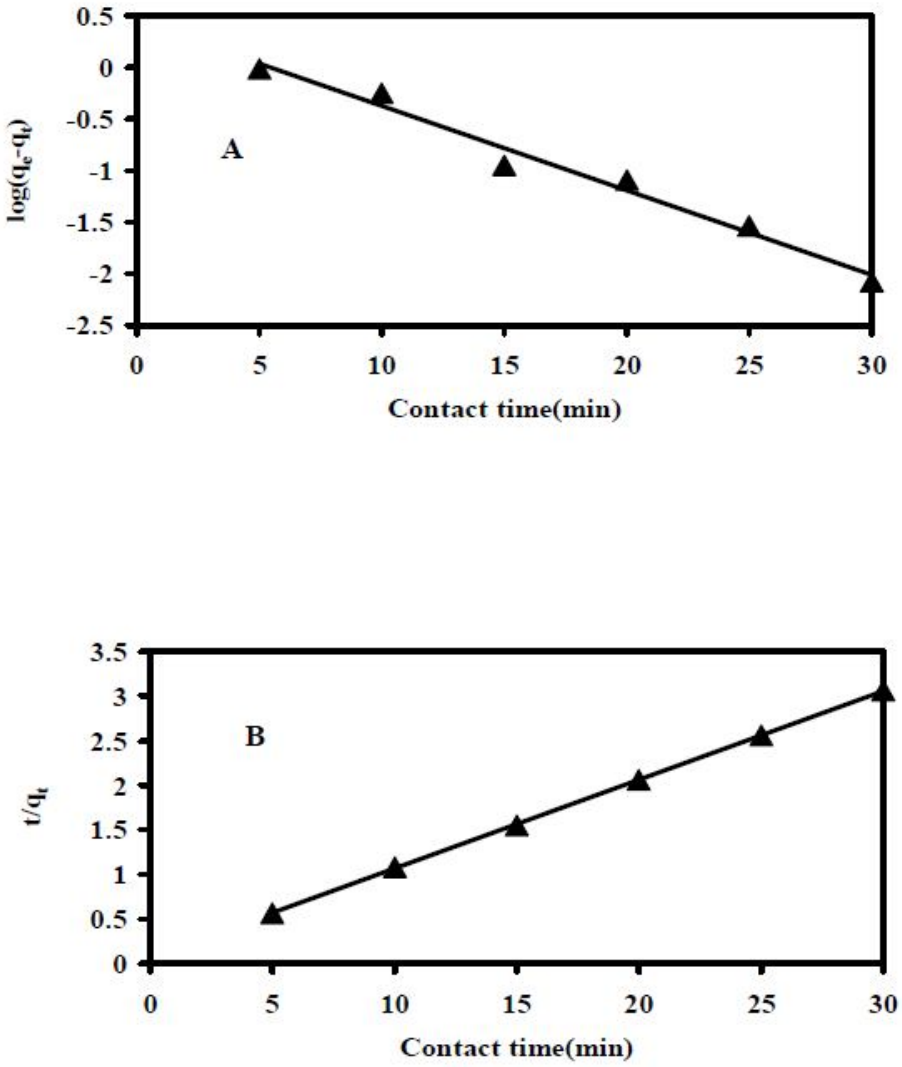

Fig. 10. (A), Pseudo-first-order; (B), Pseudo-second-order adsorption kinetics of DA onto $CoFe_2O_4$ nanoparticles.

REFERENCES

[1] R.W. Siegel, Sci. Am. 275 (1996) 74.
[2] Y.W. Jun, J.H. Lee, J. Cheon, Angew. Chem. Int. Ed. 47 (2008) 5122.
[3] M.M. Lin, D.K. Kim, A.J. El Haj, J. Dobson, IEEE Trans. Nanobioscience 7 (2008) 298.
[4] M. Namdeo, S. Saxena, R. Tankhiwale, M. Bajpai, Y. Mohan, S. Bajpai, J. Nanosci. Nanotechnol. 8 (2008) 3247.
[5] Y.W. Jun, Y.M. Huh, J.S. Choi, J.H. Lee, H.T. Song, S. Kim, S. Kim, S. Yoon, K.S. Kim, J.S. Shin, J. Am. Chem. Soc. 127 (2005) 5732.
[6] H.M. Reinl, M. Peller, M. Hagmann, P. Turner, R.D. Issels, M. Reiser, Imaging 23 (2005) 1017.
[7] G. Kenning, R. Rodriguez, V. Zotev, A. Moslemi, S. Wilson, L. Hawel, C. Byus, J. Kovach, Rev. Sci. Instrum. 76 (2005) 014303.
[8] D. Wang, J. He, N. Rosenzweig, Z. Rosenzweig, Nano Lett. 4 (2004) 409.
[9] M. Ghaemi, G. Absalan, J. Iran. Chem. Soc. 12 (2015)

Table 4. Comparison of the Performance of the Present Work with Some Reports in Literature

	Detection	Sorbent size	Modification of sorbent	Desorption solvent	Ref.
Fe_2O_3	XANES	6.5 and 3 nm	DA or AA	-	[15]
M^a/Fe_2O_3	UV-Vis	8.5 and 9.5 nm	DA-NTA	Imidazole	[16]
Metal Oxide Particles[b]	UV-Vis	<20 nm	CDB or DA or AA or AL or TBC	-	[23]
Carbon-Fiber Electrode	CV	-	2,6-AQDS or 4-Carboxyphenyl or catechols	-	[28]
Anatase TiO_2(101)	Photoemission & NEXAFS	Crystal (~3 mm × 3 mm)	DA	-	[29]
$CoFe_2O_4$	UV-Vis	10 nm	DA or AA	Imidazole	This work

XANES: Fe K-edge X-ray Absorption Near-Edge Structure, CV: Cyclic Voltammetry, CDB: dihydroxycyclobutene-dione, AA: ascorbic acid, AL: alizarin, DA: dopamine, and TBC: *tert*-butyl-cathecol, 2,6-AQDS: 2,6-Anthraquinone Disulfonic acid, NTA: Nitrilotriacetic Acid. [a]Co or $SmCo_{5.2}$. [b]TiO_2, Fe_2O_3, and ZrO_2.

1.
[10] M. Ghaemi, G. Absalan, Microchim. Acta 181 (2014) 45.
[11] M. Karimi, A.M. Shabani, S. Dadfarnia, J. Braz. Chem. Soc. 27 (2016) 144.
[12] M. Ghaemi, G. Absalan, L. Sheikhian, J. Iran. Chem. Soc. 11 (2014) 1759.
[13] C. Sun, J.S. Lee, M. Zhang, Adv. Drug Delivery Rev. 60 (2008) 1252.
[14] A. Dyal, K. Loos, M. Noto, S.W. Chang, C. Spagnoli, K.V. Shafi, A. Ulman, M. Cowman, R.A. Gross, J. Am. Chem. Soc. 125 (2003) 1684.
[15] L.X. Chen, T. Liu, M.C. Thurnauer, R. Csencsits, T. Rajh, J. Phys. Chem. B 106 (2002) 8539.
[16] C. Xu, K. Xu, H. Gu, R. Zheng, H. Liu, X. Zhang, Z. Guo, B. Xu, J. Am. Chem. Soc. 126 (2004) 9938.
[17] E. Amstad, A.U. Gehring, H. Fischer, V.V. Nagaiyanallur, G. Hähner, M. Textor, E. Reimhult, J. Phys. Chem. C 115 (2010) 683.
[18] E. Amstad, T. Gillich, I. Bilecka, M. Textor, E. Reimhult, Nano lett. 9 (2009) 4042.
[19] M.D. Shultz, J.U. Reveles, S.N. Khanna, E.E. Carpenter, J. Am. Chem. Soc. 129 (2007) 2482.
[20] H. Gu, Z. Yang, J. Gao, C. Chang, B. Xu, J. Am. Chem. Soc. 127 (2005) 34.
[21] [21] J. Xie, C. Xu, N. Kohler, Y. Hou, S. Sun, Adv. Mater. 19 (2007) 3163.
[22] J. Xie, C. Xu, Z. Xu, Y. Hou, K.L. Young, S. Wang, N. Pourmand, S. Sun, Chem. Mater. 18 (2006) 5401.
[23] T. Rajh, L. Chen, K. Lukas, T. Liu, M. Thurnauer, D. Tiede, J. Phys. Chem. B 106 (2002) 10543.
[24] H. Lee, S.M. Dellatore, W.M. Miller, P.B. Messersmith, Science 318 (2007) 426.

[25] A. Liu, I. Honma, H. Zhou, Electrochem. Commun. 7 (2005) 233.
[26] M. Gharagozlou, J. Alloys Compd. 486 (2009) 660.
[27] J. Akl, T. Ghaddar, A. Ghanem, H. El-Rassy, J. Mol. Catal. A: Chem. 312 (2009) 18.
[28] B.D. Bath, H.B. Martin, R.M. Wightman, M.R. Anderson, Langmuir 17 (2001) 7032.
[29] K. Syres, A. Thomas, F. Bondino, M. Malvestuto, M. Gratzel, Langmuir 26 (2010) 14548.
[30] C. Chinnasamy, B. Jeyadevan, O. Perales-Perez, K. Shinoda, K. Tohji, A. Kasuya, IEEE Trans. Magn. 38 (2002) 2640.
[31] M.A.M. Salleh, D.K. Mahmoud, W.A.W.A. Karim, A. Idris, Desalination 280 (2011) 1.
[32] T. Rajh, J. Nedeljkovic, L. Chen, O. Poluektov, M. Thurnauer, J. Phys. Chem. B 103 (1999) 3515.
[33] [33] P. Redfern, P. Zapol, L. Curtiss, T. Rajh, M. Thurnauer, J. Phys. Chem. B 107 (2003) 11419.
[34] L.G. Rego, V.S. Batista, J. Am. Chem. Soc. 125 (2003) 7989.
[35] B. Baeyens, M.H. Bradbury, J. Contam. Hydrol. 27 (1997) 199.
[36] S.M. Yu, A. Ren, C.L. Chen, Y. Chen, X. Wang, Appl. Radiat. Isotopes 64 (2006) 455.
[37] Z. Chen, J. He, L. Chen, S. Lu, J. Radioanal. Nucl. Chem. 307 (2016) 1093.
[38] I. Langmuir, J. Am. Chem. Soc. 40 (1918) 1361.
[39] K. Hall, L. Eagleton, A. Acrivos, T. Vermeulen, Ind. Eng. Chem. Fund. 5 (1966) 212.
[40] H. Freundlich, J. Phys. Chem. 57 (1906) 385.
[41] S. Lowell, J.E. Shields, M.A. Thomas, M. Thommes, Characterization of Porous Solids and Powders: Surface Area, Pore Size and Density, Springer Science & Business Media, 2012.
[42] A. Tóth, A. Törőcsik, E. Tombácz, E. Oláh, M. Heggen, C. Li, E. Klumpp, E. Geissler, K. László, J. Colloid Interface Sci. 364 (2011) 469.
[43] S. Lagergren, K. Sven. Vetensk.Akad. Handl. 24 (1898) 1.
[44] Y.-S. Ho, G. McKay, Chem. Eng. J. 70 (1998) 115.
[45] C. Wang, R. Yuan, Y. Chai, S. Chen, F. Hu, M. Zhang, Anal. Chim. Acta 741 (2012) 15.